Front. Optoelectron. 2012, 5(4): 358–370
DOI 10.1007/s12200-012-0285-7

REVIEW ARTICLE

Recent development in colloidal quantum dots photovoltaics

Li PENG, Jiang TANG (✉), Mingqiang ZHU

Wuhan National Laboratory for Optoelectronics, Huazhong University of Science and Technology, Wuhan 430074, China

© Higher Education Press and Springer-Verlag Berlin Heidelberg 2012

Abstract The increasing demand for sustainable and green energy supply spurred the surging research on high-efficiency, low-cost photovoltaics. Colloidal quantum dot solar cell (CQDSC) is a new type of photovoltaic device using lead chalcogenide quantum dot film as absorber materials. It not only has a potential to break the 33% Shockley-Queisser efficiency limit for single junction solar cell, but also possesses low-temperature, high-throughput solution processing. Since its first report in 2005, CQDSCs experienced rapid progress achieving a certified 7% efficiency in 2012, an averaged 1% efficiency gain per year. In this paper, we reviewed the research progress reported in the last two years. We started with background introduction and motivation for CQDSC research. We then briefly introduced the evolution history of CQDSC development as well as multiple exciton generation effect. We further focused on the latest efforts in improving the light absorption and carrier collection efficiency, including the bulk-heterojunction structure, quantum funnel concept, band alignment optimization and quantum dot passivation. Afterwards, we discussed the tandem solar cell and device stability, and concluded this article with a perspective. Hopefully, this review paper covers the major achievement in this field in year 2011–2012 and provides readers with a concise and clear understanding of recent CQDSC development.

Keywords lead sulfide, colloidal quantum dots (CQDs), solar cells, multiple exciton generation (MEG), atomic ligands

1 Introduction

As the gradual depletion of fossil fuels and the increased concern about global warming and environmental pollution, exploration of renewable energy has triggered great research enthusiasm recently. Solar energy, due to its abundance and green nature, is particularly promising as the alternative energy source. Silicon-based solar cells, including single-crystalline and multi-crystalline solar cells, had achieved an energy conversion efficiency of 25.0% and were industrially manufactured in tens of gigawatt scale in 2011. Second generation solar cells, the thin film photovoltaics, had achieved an efficiency of 17.3% (Press Release, First Solar, 26 July 2011) for CdTe and 20.3% [1] for $Cu(InGa)Se_2$ solar cell. CdTe solar cell is in mass production by First Solar and $Cu(InGa)Se_2$ solar cell is on the point of large-scale manufacturing by many companies including Solar Frontier and Nanosolar. In spite of the significant technology advancement and manufacturing cost reduction, solar generated electricity still suffers from high cost as compared with electricity generated from power plant, thus limiting its commercial competitiveness and large-scale installation.

To further reduce the cost of solar generated electricity, extensive research has focused on the third generation photovoltaics including dye-sensitized solar cell (DSSC), polymer solar cell (PSC) and colloidal quantum dot solar cell (CQDSC). We define CQDSC as the solar cells using solution processed quantum dots as the absorber materials, mainly PbS and PbSe colloidal quantum dots (CQDs). While the first two types of solar cells, DSSC and PSC, were emerged in the 1980s and experienced three decades' investigation, CQDSC is relatively new with its first report in 2005. The development of CQDSC is extremely fast within the past seven years, achieving an external quantum efficiency (EQE) of 114% [2] and an externally certified energy conversion efficiency of 7.0% [3], approaching the efficiency record of 10.6% [4] set by PSC and 12.4% [5] set by DSSC.

The fundamentals and development of CQDSC were reviewed in a few papers by Prof. Edward H. Sargent at University of Toronto, who is the leader of CQDSC research in the world. Readers are encouraged to refer to these excellent articles [6–8]. Despite the existing reviews, it would be helpful to update the researchers in the academic community with the latest development because CQDSC develops so fast that significant research progress

Received July 1, 2012; accepted August 8, 2012

E-mail: jtang@mail.hust.edu.cn

had been obtained in the past two years. We thus concentrate our discussion on the progress in year 2011–2012. In particular, this paper is organized as follows: we first discuss the advantage of CQDSCs, followed by the introduction of the CQDSCs evolution history and multiple exciton generation to provide the readers a better background understanding. We then concentrate on the latest efforts to improve device efficiency, including bulk heterojunction structure, quantum funnel design, band alignment optimization, metal contact engineering and quantum dot passivation. Afterwards, we discuss in brief the study in device stability, and conclude this review with some prospective comments.

2 Motivation for CQDSC research

Colloidal quantum dots (CQDs), particularly PbS and PbSe CQDs, are promising for the low-cost, high-efficiency third generation solar cells. Specifically, they have such kind of attractive properties:

1) Solution process enables the low-cost fabrication of CQDSCs. First, PbS and PbSe CQDs are typically synthesized by colloidal chemistry way. They are prepared through a solution-based organometallic route using PbO as the lead source, bis(trimethylsilane) sulfide or bis (trimethylsilane) selenide as the S or Se source, oleic acid as the ligand and octadecene as the solvent [9]. Second, the film fabrication is carried out at low temperature and under atmosphere pressure. After the synthesis, PbS and PbSe CQDs can be deposited onto the substrates using spin-coating, spray-coating, roll-to-to printing or ink-jet printing. This process permits high-throughput continuous manufacturing without involvement of expensive, high energy consuming vacuum-based deposition facilities. Third, flexible substrates like polymer or even paper could be used as the substrates because of its low-temperature processing. This not only initiates new applications such as wearable and bendable solar cells where flexibility is a must, but also reduces the shipment and installation cost of solar cell which constitutes a large part in the overall cost of solar generated electricity. Solution synthesis, low-temperature processing combined with flexible substrates are the three major components that contribute to the potential cost reduction of CQDSCs.

2) CQDSCs hold the potential to achieve high efficiency, even higher than the Shotkley-Queisser efficiency limit of 31% [10] for single junction solar cells. First, quantum confined states are easily observed in PbS and PbSe CQD when the particle size is smaller than its exciton Bohr radius, 18 nm for PbS and 46 nm for PbSe [11]. Using PbS as an example, the minimum transition energy limited in large dots is bounded by the bulk bandgap −0.38 eV. Due to the size tunability, the bandgap of PbS CQD ranges from 0.38 to 2.0 eV, encompassing the optimal bandgap of 1.1–1.5 eV for single junction device, 0.94 and 1.61 eV for the two-terminal tandem cell [12]. Second, multiple exciton generation (MEG), where a highly energetic photon excite multiple electron-hole pairs, is more effective in PbS and PbSe CQDs than in their bulk counterparts. MEG could significantly improve the usage of incident blue photons, yielding unprecedented EQE exceeding 100% and boosting the theoretical efficiency limit up to 44% for a single-junction solar cell [13]. More details of the MEG effect will be elaborated lately. The full absorption of solar spectrum, combined with the MEG effect, makes PbS and PbSe CQD very promising for the high efficiency photovoltaic devices.

Despite the various advantages of CQDSCs listed above, one major disadvantage, the toxicity of PbS and PbSe CQDs, need to be noted. Such toxicity concern will undoubtedly create some barriers for successful commercialization and market penetration. However, this is not an insurmountable problem if strict pollution management and products recycling are applied. As long as the CQDSCs generate electricity at a very competitive price, CQDSCs will be commercially profitable, similar to the CdTe solar panels produced by First Solar where the Cd is ten times more toxic than Pb. This argument might in part justify why people are still actively participate in the research of CQDSCs worldwide.

3 History of CQDSC development

As stated before, this paper is focused on the development of CQDSCs in the last two years. However, we will still briefly discuss the evolution history of CQDSCs, mainly in year 2005–2010, to provide readers a panoramic view of CQDSC development. In 2005, Sargent group at University of Toronto first observed the photovoltaic effect of PbS CQDs in a polymer matrix in 2005 [14]. Ever since then, CQDSCs using PbS or PbSe CQD as the active layer has been rapidly progressed. A variety of solar cell structures, including metal/CQD film, oxide/CQD film, organic layer/CQD film, and CQD/CQD film, has been explored.

In the very begging (before 2009), the simple sandwich structure of Schottky solar cells–transparent conductive oxide (TCO)/CQDs/metal had been widely studied. TCO serves as the substrates and forms Ohmic contact with CQDs. The formation of a Schottky junction between the low-work-function metal electrode and p-type CQD film creates the depletion region, where photogenerated electron-hole pairs are separated and carriers are swept to the collecting electrodes. In these days, indium tin oxide (ITO) was used as the TCO, PbS or PbSe CQDs treated with butylamine, EDT or BDT was used as the absorber layer and Ca, Mg and Al metal was used as the electrode [15]. Schottky device efficiency first exceeded 1% in 2008 from Sargent group, then improved to 2.1% by Nozik group at National Renewable Energy Laboratory (NREL)

and further improved to 3.6% by Sargent group employing pre-encapsulated PbS CQDs [16]. The simplicity and easy fabrication of Schottky solar cell is somewhat offset by the efficiency limitation mainly due to open circuit voltage (V_{oc}) deficiency. For an ideal Schottky junction, the barrier height is typically limited to ~0.67E_g, while in practical situation the V_{oc} is often lower because of defect states at the metal-semiconductor interface. The V_{oc} dependence on E_g in practical devices is observed as $V_{oc} \approx 0.49(E_g/q) - 0.253$ V [16]. In addition, the short-circuit current density (J_{sc}) in Schottky solar cells is deviated from optimal because light absorption begins at the TCO side, thus a large portion of the photogenerated carriers need to travel through the whole PbS CQD film; as a result, the recombination of carriers before electrons collection is unavoidable [8].

Because of the V_{oc} and J_{sc} deficiency associated with Schottky solar cells, CQDSCs employing heterojunction structures started to appear in 2009 and gradually dominated. Such device relies on the construction of a p-n junction where depletion region forms and the accompanied built-in field serves as the driving force for charge separation. Typical device architecture is TCO/n-type oxide/p-type CQD film/metal electrode. ITO or FTO is generally applied as the TCO, TiO_2 or ZnO as the wide bandgap n-type oxide, and high-work-function Au or Pt as the electrode. A photovoltaic device based on PbSe CQDs and ZnO film was reported with an AM1.5G efficiency of 1.6% by Norris group at University of Minnesota [17]; then Sargent group improved the device efficiency to 5.1% employing TiO_2 electrode in contact with 3-mecaptoisopropionic acid (MPA) treated PbS CQDs. We elucidate the working mechanism taking TiO_2/PbS solar cell as an example. When n-type TiO_2 contact with p-type PbS CQD film, Fermi level equilibrium necessitates the band bending and the depletion region formation at the interface. Incident light from the TiO_2 side is largely absorbed by the PbS CQD film near the interface; photoelectrons are drove into TiO_2 and photoholes are transported to the top metal electrode. Heterojunction solar cells have been shown to overcome each key limitations of Schottky junction solar cells: first, reduced interfacial defects between the oxide layer and the CQD layer releases Fermi level pinning and improves V_{oc}; second, the large discontinuity in the valence band of heterojunction device maximized shunt resistance to enhance fill factor (*FF*) and minimized back-recombination to improve V_{oc} [8]; third, most incident photons are absorbed near the junction and the collection efficiency, and consequently the J_{sc} is improved because of the shortened carrier transport distance.

4 MEG effect

The MEG effect is elucidated in detail in this section. Usually in typical semiconductors solar cells, one absorbed photon with energy larger than band gap energy excites one electron-hole pair at most and the excess energy is lost as heat, so the efficiency limit for single junction solar cell is 31% [10]. MEG is a phenomenon that one high-energy incident photon produces photocurrent with more than one electron-hole carriers. Nozik's group from NREL confirmed the MEG in PbSe CQD-based solar cells (Fig. 1(a)), which manifested an EQE peaking at 114 ± 1% and associated internal quantum efficiency of 130% [2]. MEG used to be observed spectroscopically in CQD solution with high quantum yield; while in this paper, its existence in working solar cell without external bias is confirmed. Nozik's group fabricated the solar cells employing the simple planar heterojucntion structure ITO/ZnO/PbSe CQD/Au. PbSe CQD film was treated with 1,2-ethanedithiol (EDT) and hydrazine to remove the long-chain oleate ligand while maintain or improve surface passivation. The EQE curves (Fig. 1(b)) showed that the best performing device collected 1.14 pair of photocarriers per absorbed incident photons at the energy of almost 4 times of band gap energy. They observed the MEG threshold for PbSe CQD is 2.61E_g with an efficiency of 0.62, as compared to the MEG efficiency of only 0.31 and the corresponding threshold energy of 4.22E_g in bulk PbSe. This low MEG threshold energy also compares favorably with bulk silicon (3.5E_g) and germanium (4.1E_g) based solar cells. Even though there was no breaking record efficiency of devices, this was the first observation of EQE exceeding 100% in realistic solar cells, providing the direct evidence that MEG could serve as a path to achieve high efficiency photovoltaics.

5 Efforts to improve device efficiency

The function of solar cell is to convert solar radiance into electricity. Naturally, it is preferred that maximum incident light is absorbed by the solar cells. Since the absorption coefficient of PbS and PbSe CQD film at their band edge is approximately 10^4 cm^{-1}, simple calculation indicated that absorption of $> 90\%$ incident sunlight necessitates ~ 1 μm thickness. Once the light is absorbed, photogenerated carriers need to be collected by the electrode to power the external load. Carriers generated inside the depletion region could be easily swept outside by the residing electrical field. Carriers generated inside the quasi-neutral region, plus the carriers drifted to the quasi-neutral region, need to diffuse to their destination electrode. The depletion region, or equivalently the drift length, is around 100–200 nm in typical CQDSC devices depending on their doping density and dielectric constant; the diffusion length, which is correlated to carrier mobility and lifetime, is around 50–100 nm in typical CQDSC devices [8]. A large gap presents between the optical length (film thickness required for full light absorption) and the effective carrier

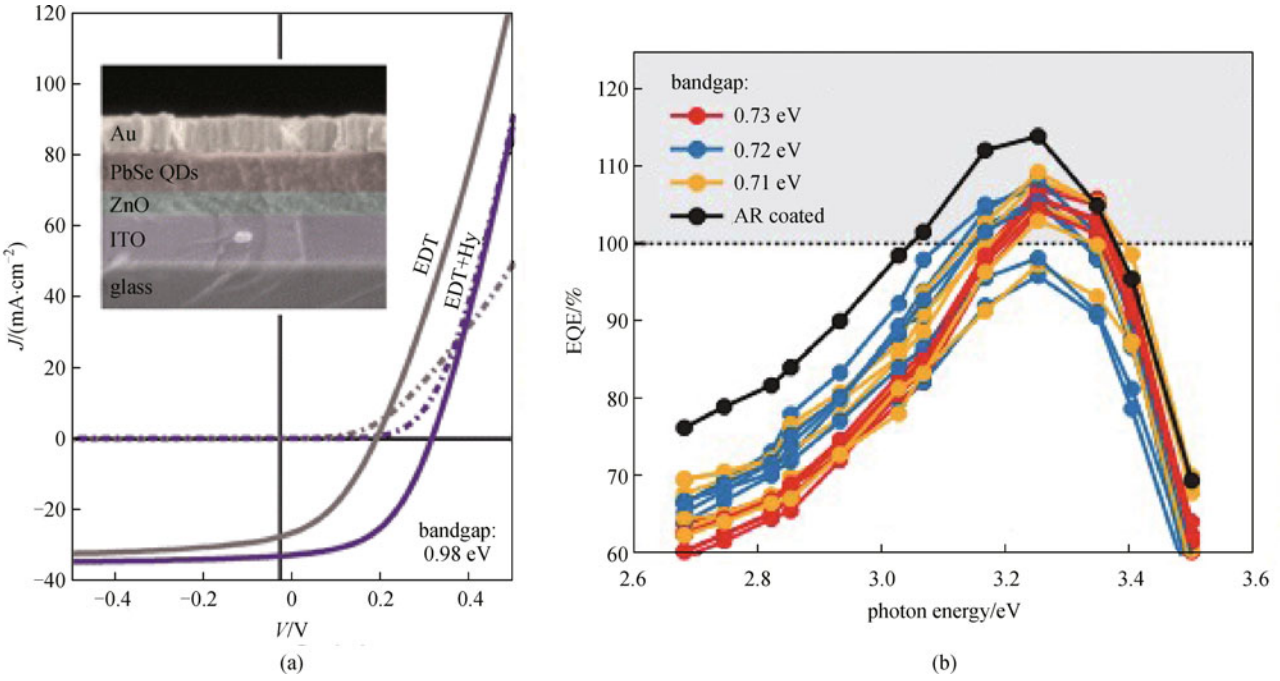

Fig. 1 (a) *J-V* characteristics of devices assembled from EDT– and EDT + hydrazine (Hy)–treated 0.98 eV PbS CQDs film (the inset figure displays a false-color cross-sectional SEM of a typical device); (b) EQE peaks for 18 independent devices made with CQDs bandgaps of 0.71 eV (yellow), 0.72 eV (blue), and 0.73 eV (red), and a device with an antireflective (AR) coating (black) (reprinted from Ref. [2])

collection length (depletion width plus diffusion length). Furthermore, photogenerated carriers are prone to recombine within the defects inside the CQD film, a loss mechanism that contributes to the reduced photocurrent. Besides, the contact electrode should be perfectly Ohmic; once there is a barrier at the CQD/electrode interface, carrier will be blocked leading to significant carrier collection loss. Researchers are well aware of all these loss pathways and various strategies are proposed and implemented to overcome these problems. These strategies are the major emphasis of this review paper and will be discussed in detail in the following section.

5.1 Bulk-heterojunction architecture

As stated above, absorbing lights and efficiently collecting carriers are both significant for the device performance. Thicker active layers absorb more light to excite more photocarriers, but require the carriers to transport longer distance to the collecting electrode during which more recombinations are prone to occur. To balance those two aspects and overcome the insufficient collecting obstacles, bulk heterojunciton architecture is applied in recent device optimization.

Bulk heterojunction is not a novel concept; it is already widely adopted in polymer solar cells. The basic idea is to mix electron-donating material and electron-accepting material on a length scale of tens of nanometers. In CQDSC, the diffusion length of carriers is far less than the drift length. To enhance the advantage of longer drift length, bulk heterojunction CQDSC with increased active layer volume for light absorbing while maintaining the efficient carrier collection, emerged as the efficiency required. Barkhouse et al. from University of Toronto had reported the first solution-processed depleted bulk heterojunction (DBH) solar cells with EQE of 40% at their 950 nm excitonic peak and efficiency of 5.5% under simulated AM1.5 illumination [18]. The devices were built by stacking large TiO_2 nanoparticles (150–200 nm diameter) on top of a compact TiO_2 layer composed of small TiO_2 nanoparticles to form a porous TiO_2 electrode, then infiltrated with spin-coated PbS CQD layer. The idea of using porous TiO_2 was further developed by Kramer et al., who presented a well-structured TiO_2 nanopillar electrode with a defined spacing, height and aspect ratio, and employed it to the DBH CQDs solar cells [19]. As shown in Fig. 2, the TiO_2 electrodes were molded as uniform nanopillars with a peak-to-peak distance of approximately 275 nm. This distance was determined by the length of depleted region in the best CQDs films and diffusion length of minority carriers. In such structure, photoelectrons would be generated in the depleted region, drifted to the TiO_2 and were efficiently collected. Because of the nanopillar structure, DBH solar cells enjoyed a much improved J_{sc} of 20.1 mA/cm^2 from 16.1 mA/cm^2 in the planar control devices, and an AM 1.5 efficiency of 5.6%

was achieved. In summary, the key point to form the DBH structure is to increase the thickness of the CQDs film and ensure that the whole CQDs film is depleted, thus increasing the light absorbance especially in infrared (IR) regions without sacrifice of carrier collection efficiency. Consequently, EQE is significant improved leading to better device efficiency.

The above mentioned DBH structure solar cells adopt traditional n-type material TiO_2, which is a wide bandgap oxide semiconductor contributing very little to light harvesting. Additionally, the high temperature annealing is incompatible with flexible polymer substrates. Rath et al. at the Institute of Photonic Sciences in Spain first applied a solution-processed Bi_2S_3 layer, which is a non-toxic material with a favorable band gap of 1.3 eV, as the n-type electron acceptor to build CQDSCs [20]. These solar cells adopting solution-processed Bi_2S_3 achieved 1.6% efficiency using 860 nm PbS CQDs and over 1% efficiency using 1300 nm PbS CQDs. Based on this work, they further raised a new concept –bulk nano-heterojunction (BNH): n-type Bi_2S_3 and p-type PbS CQDs were mixed in solution and then spin-coated into a CQD composite film. In such way, a bulk heterojunction was formed in nanoscale prolonging the carrier lifetime [21]. As shown in Fig. 3, the BNH solar cells were composed of three different layers: a bottom layer of PbS CQDs, an intermediate layer of blend (PbS and Bi_2S_3 CQDs) and a top layer of Bi_2S_3 CQDs. The optimal BNH film was found to be 180 nm thick with a PbS to Bi_2S_3 weight ratio of 1:2. The best performing BNH device achieved 4.87% device efficiency, as compared to the 1.46% planar control device. The improvement was solely from the J_{sc} gain with a threefold improvement, being 24.2 mA/cm^2 for the BNH device and 6.81 mA/cm^2 for the control device. In the BNH device, a continuous percolation path was formed to allow for efficient charge transport: PbS CQD path for holes and Bi_2S_3 CQD path for electrons. Once separated at the p-n junction interface, both electrons and holes traveled as the majority carriers in their respective pathways, thus minimizing the recombination loss. The BNH concept provides a new and attractive strategy for nanoparticles-blend-based optoelectronic and photovoltaic devices.

In summary, the bulk heterojunction strategy, including the DBH and the bulk nanoheterojunction structure, targets at full absorption of incident light while maintain efficient charge collection. This is achieved by integrating the p-

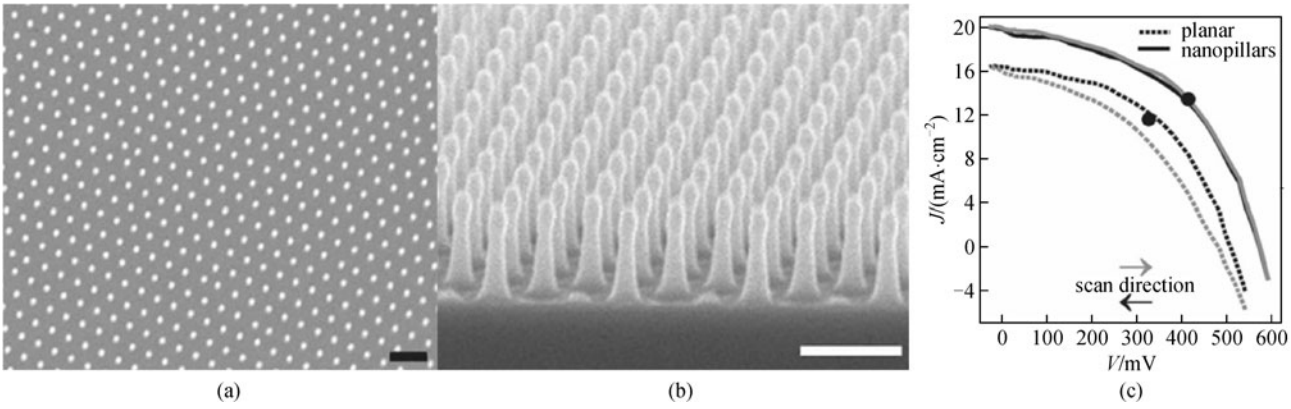

Fig. 2 SEM of (a) top and (b) angled side view of titania nanopillar on FTO-coated glass substrates. The scale bars are 500 nm. (c) *J-V* curves of planar and nanopillar devices showing $\eta = 5.6\%$ for nanopillar architecture (reprinted from Ref. [19])

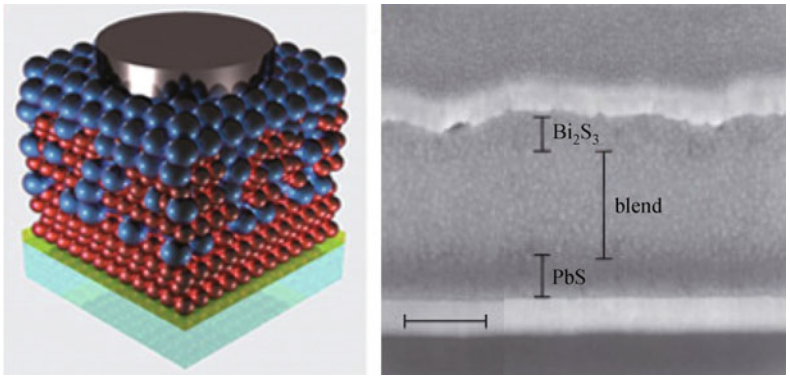

Fig. 3 Schematic of BNH device structure consisting of ITO/PbS CQDs/PbS, Bi_2S_3 nanocomposite /Bi_2S_3 nanocrystals/Ag and cross-sectional SEM image with scale bars: 200 nm (reprinted from Ref. [21])

type and the n-type materials into a percolated but individually continuous network. Photogenerated carriers efficiently separate at the junction interface, and then quickly move through the network to the collecting electrodes. Charge separation and transport are significantly improved, leading to better device performance.

5.2 Quantum funnel

Bulk heterojunction design provides a tactful approach to improve carrier collection by minimizing the distance that photogenerated carriers need to diffuse to the electrodes. Quantum funnel strategy, the strategy to stack PbS or PbSe CQDs of different size to form the film, providing an attractive alternative to boost carrier collection. Because of the quantum confinement, CQDs of different size have different band gaps and consequently different band positions. In addition, CQDs film is built from layer-by-layer spin-coating, a process that CQDs of different size could be easily integrated. By stacking layers of CQDs with designed size and fashion, cascade- or funnel-like band alignment will form within the film, facilitating charge transport within the CQD film, namely from the small CQDs to the large CQDs. Xu et al. at University of Delaware had introduced multilayered cascaded PbS CQDs superstructure using monolayers of CQDs with different sizes to form the grading band gap [22]. In their experiment, they used EDT and 1,3-benzenedithiol (BDT) treated PbS CQDs of different sizes and found efficient exciton funneling and recycling of surface state-bound excitons. Excitons transferred from small PbS CQDs or donor layers to larger PbS CQDs or acceptor layers, as evidenced by the dramatically improved photoluminescence from the acceptor layers.

At the same time, Kramer et al. at University of Toronto further implemented the quantum funnel concept into realistic devices [23]. In their report, PbS CQDs of 4.3, 4.2 and 4.0 nm treated with MPA were subsequently deposited onto TiO_2 to build the graded device. Bandgap engineering with the light-absorbing, charge-transporting CQDs active layer to funnel photoelectrons to the charge-collecting TiO_2 electrode was exploited in this paper, benefiting from enhanced *FF*. Figure 4 showed three types of device structure: ungraded, graded and anti-graded PbS active layer and the band gap diagram of different-size PbS CQDs. Device performance measurement indicated the improvement mainly came from J_{sc} and *FF*: for the graded device, the J_{sc} and *FF* is 11.2 mA/cm^2 and 47%; while for the ungraded device, the J_{sc} and *FF* is 10.7 mA/cm^2 and 39% and for the antigraded device, the J_{sc} and *FF* is 10.2 mA/cm^2 and 31%, respectively. Photoluminescence experiment further confirmed funneling phenomenon occurred that when illuminated from its large-band gap CQD side, the graded device emitted photoluminescence exclusively from its small-band gap, larger CQDs. In conclusion, quantum funnel strategy, taking advantage of the easy tuning of band position in CQDs film by quantum confinement, provides an additional driving force to assist charge transport within the CQD film. Device performance was improved in terms of J_{sc} and *FF* due to better carrier transport and collection.

5.3 Band alignment optimization

Both bulk heterojunction and quantum funnel strategies provide methods to effectively drive carriers toward the junction interface where electron-hole separation. Proper band alignment at the junction is crucial for charge separation and hence device performance. As shown in Fig. 5, when the conduction band of PbS CQDs is lower than TiO_2, J_{sc} is less than optimal because electron needs to overcome the energy barrier to inject into TiO_2 layer, but the V_{oc} is maximized due to the large separation between the quasi-Fermi level of electrons in TiO_2 and quasi-Fermi level of holes in PbS CQDs film. When the conduction band of PbS CQDs is higher than TiO_2, electron injection into TiO_2 layer is facilitated but at the price of poor V_{oc}. Only when the band alignment between PbS CQDs and TiO_2 layer is perfectly match, both J_{sc} and V_{oc} would be optimized leading to best device efficiency. Guided by this understanding, Liu et al. at University of Toronto studied doping of TiO_2 electrode to tune its conduction band in the

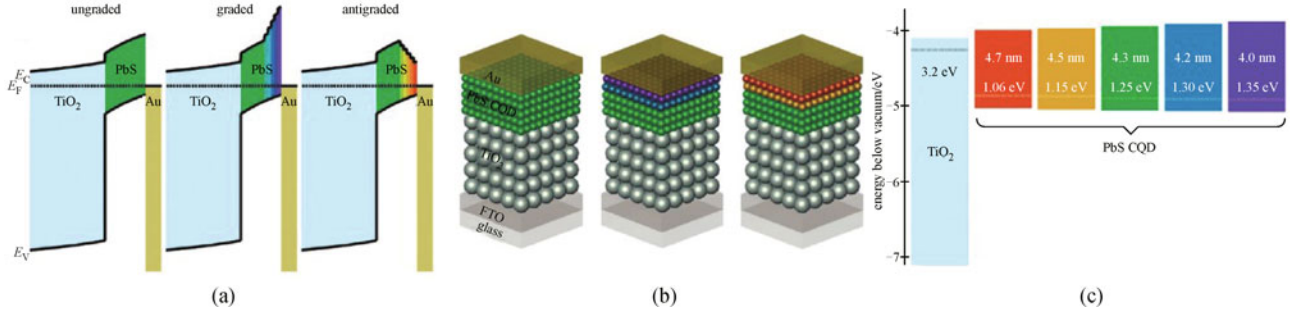

Fig. 4 (a) Spatial band diagrams of ungraded, graded and antigraded CQDs solar cells; (b) schematic diagram of device cross sections; (c) detailed band alignment for TiO_2 and PbS CQDs materials used. All color coding corresponds to larger bandgaps (more blue/violet) and smaller bandgaps (more yellow/red) (reprinted from Ref. [23])

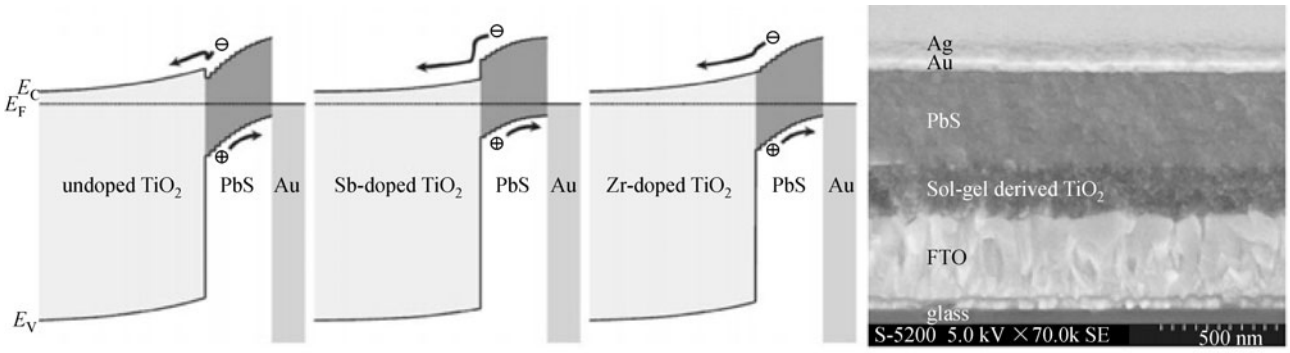

Fig. 5 Schematic band diagram of DH-CQD devices at equilibrium: Zr-doped TiO_2 shows the optimal band alignment that combines maximal charge separation with high open-voltage; and the cross-sectional SEM image of the device (reprinted from Ref. [24])

hope of optimally aligning the band between TiO_2 and PbS CQDs film [24]. Many dopants were tried to be included into TiO_2, and Zr doping showed promising improvements in CQDs photovoltaic performance: device employed Zr doped TiO_2 electrodes achieved 5.6% efficiency under simulated AM1.5 illumination with a J_{sc} of 19 mA/cm^2, while the device employed undoped TiO_2 electrode had an efficiency of 3.8% with a J_{sc} 16.1 mA/cm^2. Field effect transistor (FET) measurements eliminated the difference in electron mobility and concentration between doped TiO_2 electrodes, and cyclic voltammetry study revealed that Zr doping yield TiO_2 electrode had the conduction band at −3.95 eV, best matching the 950 nm PbS CQDs employed in the device fabrication. Optimal band alignment resulted in balanced V_{oc} and J_{sc}, providing the best performing device.

5.4 Metal contact engineering

Since p-type PbS or PbSe CQD film is exclusively applied to build CQDSCs, high-work-function metal like Au and Ag is adopted for the top metal contact. Ohmic contact is always preferred for this contact to minimize the interfacial barrier and ensure 100% carrier collection. Gao et al. from NREL studied the *J-V* characteristics of ITO/ZnO/PbS CQD/metal devices and found the roll-over (current saturation at high forward bias) and crossover (intersection of dark and light current under forward bias) effect. They ascribed this behavior to the presence of a Schottky barrier at the PbS CQD/metal interface, which is dependent on the size of CQDs and the work-function of the metal contact [25]. The Schottky-barrier height related closely to the CQDs size: for a given metal contact, CQDs diameter decrease led to the holes extraction barrier increase.

Following these findings, Gao et al. introduced the n-type transition metal oxide (TMO) consisting of molybdenum oxide (MoO_x) and vanadium oxide (V_2O_x) as the hole extraction layer (HEL) [26], a concept that was previously used in organic LEDs and organic solar cells. Device structure ITO/ZnO/PbS CQD/TMO/Au was showed in Fig. 6(a). ZnO nanocrystal layer was spin-coated to the clean substrate ITO; PbS CQDs layer was dip-coated using EDT treatment, and the TMO layer and metal anode was produced by thermal evaporation. Experiments showed that without TMO layer, device performance varied with different anode, Au being better than Ag because of its higher work function showed better performance; while with TMO layer, cell performance kept consistent regardless of metal contact used. This is explainable by an interfacial dipole formed between PbS CQD and MoO_x layers. As shown in Fig. 6(b), the interfacial dipole increased the work function of PbS CQDs to 5.0 eV, allowing more efficient hole colelction at the PbS/MoO_x interface. ZnO/PbS CQD device using MoO_x/Al contact had a NREL certified device efficiency of 4.40%: V_{oc} of 0.524 V, J_{sc} of 17.9 mA/cm^2 and *FF* of 48.7%.

In parallel, Brown et al. from MIT also reported that incorporation a MoO_3 interlayer between the PbS CQDs film and the top-contact anode significantly increased device performance in all aspects including V_{oc}, J_{sc} and *FF* [27]. Combination of different measurements showed that the key reason for the enhancement was due to the elimination of a reverse-bias Schottky diode presented at the PbS/anode interface: the high work function of MoO_3 layer pin the Fermi level of the top electrode, changing the formation of Schottky contact to Ohmic contact. Additionally, MoO_3 layer acted as a physical protective layer for the underlying PbS during deposition of top electrode. The beneficial effect of MoO_3 layer for hole collection was further confirmed by Jeong et al. when built CQDSCs using extremely small PbS CQDs (E_g = 1.6 eV) [28], and also confirmed by Klem et al. from RTI International who found that a discontinuous 1 nm MoO_3 layer sandwiched between the ITO and the PbS CQD layer significantly improved device efficiency up to 5.2% [29].

All the examples discussed above showed that n-type MoO_3 could work as efficient hole-collecting layer in CQDSCs. When sandwiched between PbS CQD film and metal electrode, Ohmic contact was produced independent of metal work function. Due to its perfect hole- collecting

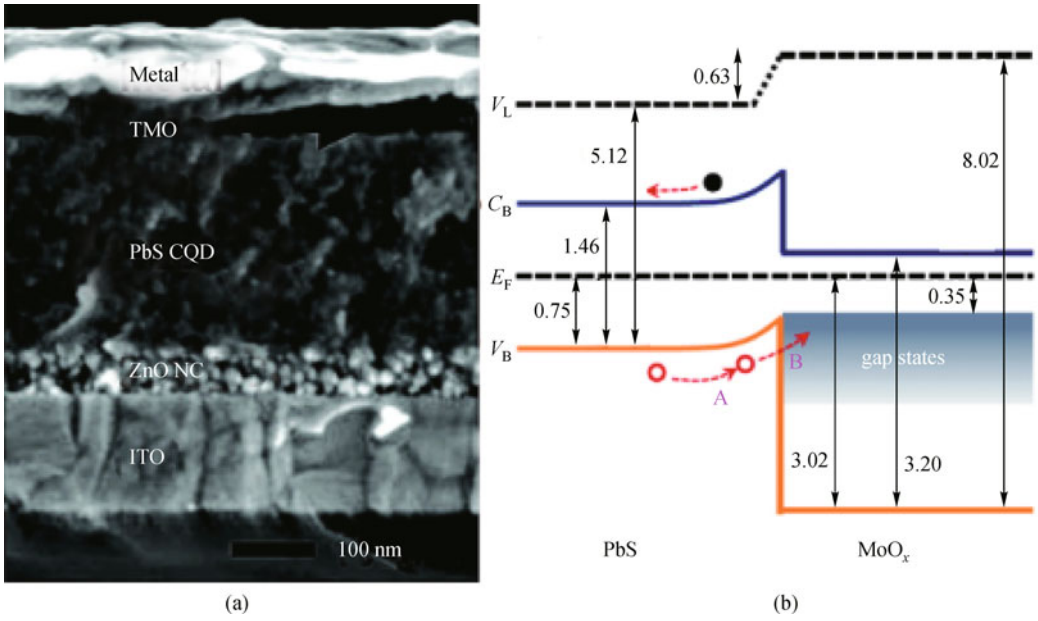

Fig. 6 (a) Cross-sectional SEM image of typical PbS CQDs solar cells with TMO; (b) schematic energy diagram of interfacial layers PbS/MoO_x deduced by the UPS data (reprinted from Ref. [26])

and low-cost characteristics, MoO_3/Al is widely accepted as the optimal Ohmic electrode contacting p-type PbS and PbSe CQD film.

5.5 Quantum dot passivation

Previous discussion is mainly focused on the optimization of device configuration; now we discuss recent progress in CQD passivation in the context of CQDSC application. CQD film is the active layer which absorbs incident light, generates electron-hole pairs and transport carriers to the electrodes. It is built through a layer-by-layer spin-coating or dip-coating process, during which a solid-state ligand exchange is applied. Historically, short organic ligands, such as EDT, BDT and MPA, were generally used. These ligands have dural roles: they strip off the original long oleate ligand and reduce the interparticle distance to boost carrier mobility; they passivate surface defects associated with dangling bonds to reduce trap density and depth. Enhanced carrier mobility, in conjunction with low trap density and shallow trap depth is the key to achieve high performance CQDSCs. All these parameters are determined by the choice of ligands and the processing of ligand exchange. In this section, we will review the new ligand chemistry: atomic ligands and hybrid passivation.

Tang et al. at University of Toronto first introduced atomic ligand, namely, halide anions, to passivate PbS CQDs and fabricate CQDSCs [30]. As shown in Fig. 7, a two step passivation strategy was applied: $CdCl_2$-tetradecylphosphonic acid (TDPA)-oleylamine (OLA) complex was introduced into pre-synthesized PbS CQDs to passivate the sulfur anions on CQD surface; then cetyltrimethylammonium bromide (CTAB) methanol solution was applied to remove the oleate ligand and passivate surface cations during the layer-by-layer film fabrication procedure. In short, Cd^{2+} was introduced to passivate S^{2-} and Br^- to passivate Pb^{2+} on PbS CQDs surface. Since both cations and anions were well passivated, surface defects and consequently trap density were substantially reduced. Moreover, Br^- is monovalent and the shortest ligand which gives rise to close CQD packing and significant mobility improvement. As revealed by time-resolved infrared spectroscopy and field effect transistor measurements, bromide passivated PbS CQDs exhibited ten times reduction in trap density and one hundred times improvement in carrier mobility as compared to conventional EDT treatment. They applied this passivation strategy to build a heterojunction solar cell FTO/TiO_2/PbS CQD/Au and achieved an externally certified device efficiency of 5.1%: V_{oc} of 0.544 V, J_{sc} of 14.6 mA/cm^2 and FF of 62%. In addition to Br^-, devices using other halide or pesudo-halide anions such as Cl^-, I^- and SCN^- all yield decent device performance. This atomic passivation strategy, implemented in ambient using inexpensive chemicals, demonstrated its strength to produce CQD film with high carrier mobility and low defect concentration, suggesting its potential application for other optoelectronic devices based on CQDs.

Ip et al. further developed this atomic ligand strategy to hybrid passivation in which both atomic ligand (Cl^-) and organic ligand (MPA) were applied to treat the PbS CQDs, as shown in Fig. 8 [3]. Density function theory simulation revealed that MPA molecules could not access all the interatom trenches on PbS CQD surface because of steric

hinderance or lack of appropriate coordination number, thus leaving unpassivated surface defects acting as detrimental mid-gap states. Small Cl^- anion, however, could access to these trenches and multiply cordinate to eleminate the mid-gap states. Experimentally, Cl^- binding was carried out in solution by injection $CdCl_2$-TDPA-OLA complex during the end stage of PbS CQD synthesis; MPA treatment was applied in solid state to remove the insulating oleate ligand and gurantee close packing. Following such a hybrid passivation strategy, all surface defects on CQD surface were well passivated, leading a charge-balanced CQDs with minimal trap states. Density of state within the band gap measured from photovoltage transient technique, hole mobility revealed by time of flight

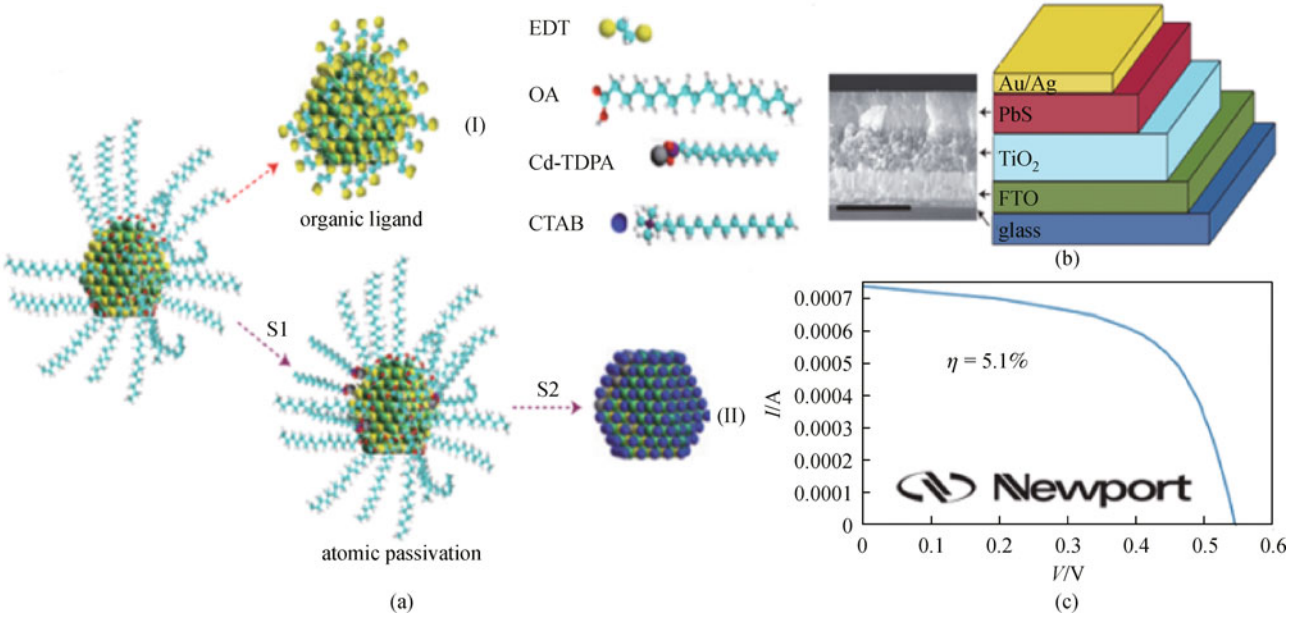

Fig. 7 (a) Schematic comparison of organic and atomic passivation strategies; (b) structure diagram and cross-sectional SEM; (c) *I-V* curve with V_{oc} = 0.544 V, I_{sc} = 0.00071 A, FF = 62% and η = 5.1% (reprinted from Ref. [30])

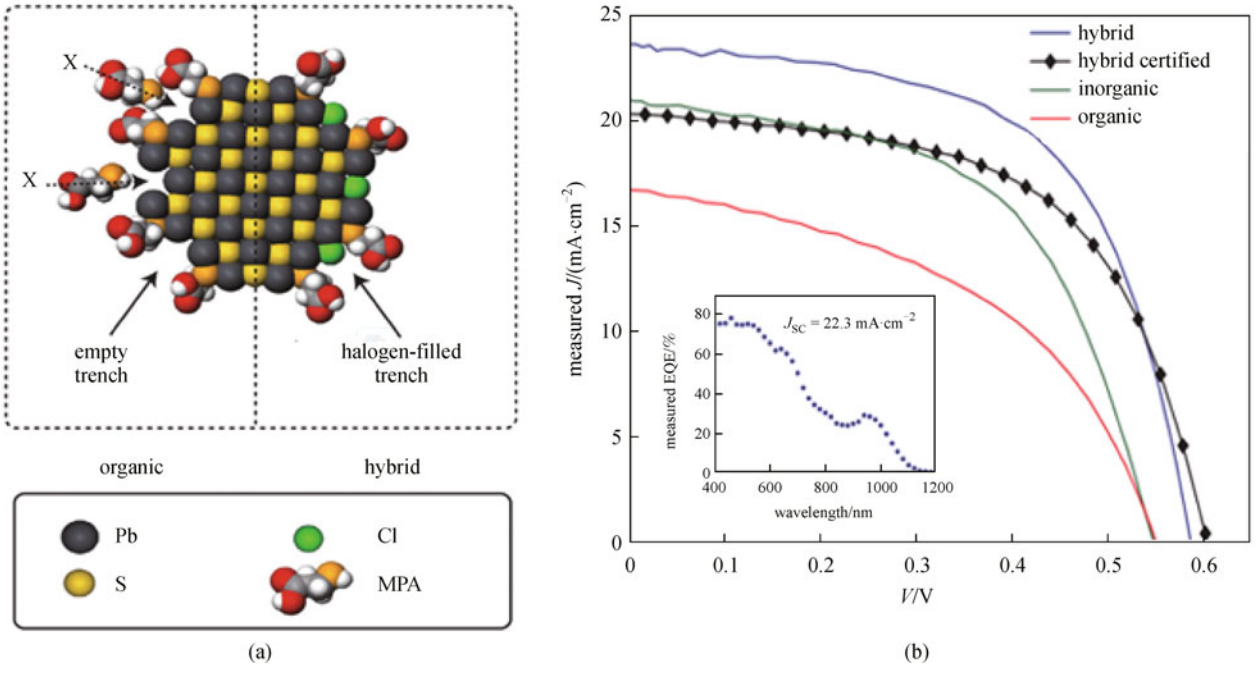

Fig. 8 (a) Schematic cross-section of PbS CQD with organic passivation (left) based on MPA, alkanethiol, and hybrid passivation scheme (right); (b) *J-V* curves. Black diamonds are *J–V* curve for hybrid passivated device as measured by Newport. Inset: EQE curve for hybrid passivated device (reprinted from Ref. [3])

characterization, as well as theoretical simulation all confirmed the substantial reduce in mid-gap state in PbS CQD film using hybrid passivation. This is further confirmed by the fact that the heterojunction solar cell, FTO/(ZnO/TiO_2)/PbS CQD/MoO_x/Au/Ag using Cl^- and MPA hybrid passivation, achieved a Newport certified AM1.5 efficiency of 7.0%: V_{oc} of 0.605 V, J_{sc} of 20.1 mA/cm^2 and *FF* of 58%. This is the efficiency record of CQDSCs so far, fully demonstrating the strength of hybrid passivation.

From the above two examples, it is apparent that quantum dot passivation leads to devices with best performance. CQD film is the absorber layer of the CQDSC and its poor carrier mobility and high defect concentration limits device performance. Not surprisingly, atomic ligand and hybrid passivation, both of which are very effective in CQD passivation, improved the quality of CQDs film and manifested the best efficiency gain.

6 Tandem solar cells

Building multiple-junction devices is a strategy to achieve power conversion efficiency higher than the Shockley-Queisser limit. The theoretical efficiency limit for double-junction (tandem) and triple-junction solar cell is 42% and 49%, respectively [31]. Tandem solar cell is two devices connected in series: the top cell consisting of semiconductor with large E_g to absorb incident blue light, the bottom cell consisting of semiconductor with smaller E_g to absorb the red light passing through the top cell. The overall output voltage is the summation of voltage from each individual cell; and the overall output current is the smaller one generated in individual cells. Because the two sub-cells are connected in series, two key requirements need to be satisfied to fabricate efficiency tandem solar cells:

1) Current match: the top and bottom solar cell should approximately absorb the same amount of photons and generate the same amount of electron-hole pairs when incident light illuminates the tandem solar cell. Based on this principle, the optimized band gap is 1.6 and 1.0 eV for top and bottom cells, respectively; and the film thickness needs to be customized according to their absorption coefficient.

2) High quality intervening layer: photoelectrons form the one sub-cell and photoholes from the other sub-cell should combine in the intermediate layer. The design of this layer significantly affects the performance of tandem solar cells. It should be optically transparent to pass light to the bottom cell; and should provide proper energy level alignment to accept electrons and holes without degrading the overall photovoltage.

CQDs are very suitable for tandem solar cells because their band gap could be easily tuned through quantum confinement. Small CQDs with large band gap could be used for the top cell, and large CQDs for the bottom cell. Wang et al. from University of Toronto demonstrated the first tandem colloidal quantum dot solar cells with an open circuit voltage of 1.06 V and an efficiency of 4.2% [32]. The device structure is ITO/TiO_2/1.6 eV PbS CQD/graded recombination layer (GRL)/1.0 eV PbS CQD/Au/Ag. Light was illuminated from the ITO side and hence we define this side as the top. Both PbS CQDs layers were fabricated by spin-coating using MPA treatment and the thickness was well-controlled to ensure current match. The GRL was deposited by sputtering progress at room temperature. GRL was applied as the intervening layer to achieve barrier-free conveyance of electrons from the bottom cell to recombine with the holes from the top cell. The GRL concept overcame the large energetic barrier introduced by directly connection of deep-work-function contact of the top cell with the shallow-work-function electron-acceptor of the bottom cell by using a progression of work functions from the top to the bottom: deep-work-function n-type MoO_3, ITO and shallow-work-function with heavily doped aluminum-doped zinc-oxide (AZO), without adding appreciably to the series resistance. The solar cell structure and band diagram was showed in Fig. 9. The top subcell had a V_{oc} of 0.70 V, and the bottom subcell of 0.39 V. The tandem solar cell exhibited a V_{oc} of 1.06 V, equaling, within a few percent, to the sum of the V_{oc} of single junction subcells, confirming the efficiency of GRL. It should be noted that Choi et al. from Cornell University also fabricated a tandem CQDSCs by employing a ultrathin Au layer and a p-type poly (3,4-ethylenedioxythiophene):poly (styrenesulfonate) (PEDOT:PSS) layer as the interlayer to connect CQDs-based subcells [33]. In their tandem solar cell, they achieved a V_{oc} of 0.91 V while the subcell V_{oc} was 0.58 and 0.32 V, respectively; and the best device efficiency is 1.27%.

A further work was done by Koleilat et al. to generalize conditions for design of efficient GRL in tandem solar cells [34]. In their paper, they focused on the number of interlayers and the requirements on work function and doping of each interlayer. They found that to bridge top cell with bottom cell in tandem structure, a single optimal work function interlayer was sufficient with a relatively high doping density of 1×10^{19} cm^{-3}; a pair of interlayers with much lower doping density of 1×10^{16} cm^{-3} could span the energy differences as large as 1.0 eV.

7 Stability

The ultimate goal of CQDSC research is to generate high efficiency, low cost and stable solar cells. For real applications, stability is at least as important as efficiency. Commercial photovoltaic modules must survive the harsh test of 1000 h soaking at 85°C with 85% relative humidity. As CQDs are intrinsically metastable materials due to their large surface-to-volume ratio and high surface energy, oxidization and photothermal degradation is always a big concern. Following the pioneer work of stability engineer-

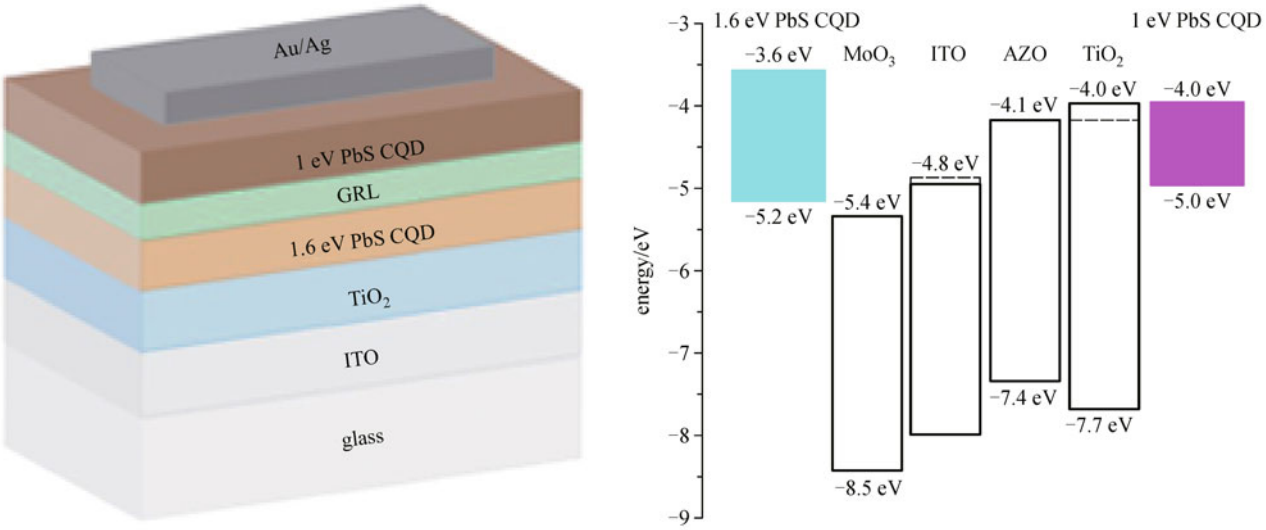

Fig. 9 Device structure of CQDs based tandem solar cells and energy level diagram showing HOMO and LUMO energies of each type of PbS CQDs, the Fermi levels (dashed lines) and band edges of isolated GRL materials (reprinted from Ref. [32])

ing using small PbS CQDs processed under ambient atmosphere [35,36], Luther et al. at NREL demonstrates a 3% bilayer ZnO/PbS CQDSCs device which was stable under 1000 h of continuous illumination in ambient air without encapsulation [37].

The 1000 h stability of ZnO/PbS CQDSC is encouraging, and researchers continued their effort in stability improvement. Liu et al. at University of California, Irvine carried out very careful and detailed study to investigate the effect of ultraviolet light, heat treatment and ambient oxidation on the stability of PbS and PbSe CQDs film [38]. Two systems, EDT treated PbS CQDs and BDT treated PbSe CQDs were chosen for study, and optical absorption spectroscopy, transmission electron microscopy and field effect transistor measurement were applied for characterization. They found out surface oxidation, diffusion, ripening and sintering all contributed to the instability of PbS and PbSe CQD solid. They observed, for example, aging PbS CQDs in ambient atmosphere caused oxidation and blue shifts of excitonic peak; aging in N_2 however, resulted in ripening/sintering of PbS CQDs and red shifts of excitonic peak. They also observed that UV illumination caused preferential oxidation of large PbS CQDs but preferential ripening/sintering of small CQDs.

Based on this observation, Liu et al. further introduced atomic layer deposition (ALD), a stepwise chemical vapor deposition technique, to infill a thin conformal amorphous Al_2O_3 into PbS and PbSe CQD film [38]. ALD deposited Al_2O_3 layer created a diffusion barrier between adjacent PbS or PbSe CQDs, locking CQDs in place against oxidization and sintering. The inorganic matrix, as compared to the original organic ligand, also reduced the inter-CQD tunnel barrier size, thereby increasing the film mobility. As a result, CQDSC devices filled and overcoated with amorphous Al_2O_3 layer not only retained more than 95% of their performance after 1 month of storage in air (the untreated devices degraded within hours in air to ~30% of their original efficiency); but also exhibited significantly increased V_{oc}, J_{sc} and FF with typically twice the conversion efficiency of control devices without Al_2O_3 coating. Apparently, encapsulating CQDs with an inorganic matrix through ALD process showed excellent potential to protect PbS and PbSe CQDs against oxidation and photothermal damage, leading to devices with long-term stability.

8 Conclusions and perspective

The efficiency of CQDSC steadily increased since its first report in 2005, being approximately 1% per year. Such a soaring efficiency improvement rooted from the improved device structure, from Schottky to depleted heterostructure and to bulk depleted heterostructure or bulk nanoheterostrcuture. The efficiency improvement also benefit significantly from the ligand optimization, from oleate to short organic thiols, then to atomic ligands and recently to hybrid passivation. Architecture and film quality optimization are the two major driving forces that boost the CQDSC efficiency from 5% in 2010 to 7% in 2012. As our understanding toward the carrier generation, separation, transport and annihilation within CQDs film deepens, the quality of CQDs film and the efficiency of CQDSC efficiency will further improved. Hopefully, the 1% per year momentum will continue. In addition, device degradation mechanism needs careful characterization to improve the device stability, especially the operational lifetime. A combination of module efficiency of 10% produced through the solution process, with an operational lifetime of at least five years, probably will overcome the

Pb toxicity issue and make this technique commercially viable.

Acknowledgements J. Tang acknowledges the guidance and supervision of Prof. Edward H. Sargent during his Ph.D study. It is the experience and knowledge gained in Prof. Sargent's group that makes this review possible. J. Tang also acknowledges Prof. Guozhen Shen at Wuhan National Laboratory for optoelectronics, Huazhong University of Science and Technology, for his help and support during the manuscript preparation.

References

1. Jackson P, Hariskos D, Lotter E, Paetel S, Wuerz R, Menner R, Wischmann W, Powalla M. New world record efficiency for Cu(In, Ga)Se_2 thin-film solar cells beyond 20%. Progress in Photovoltaics: Research and Applications, 2011, 19(7): 894–897
2. Semonin O E, Luther J M, Choi S, Chen H Y, Gao J, Nozik A J, Beard M C. Peak external photocurrent quantum efficiency exceeding 100% via MEG in a quantum dot solar cell. Science, 2011, 334(6062): 1530–1533
3. Ip A H, Thon S M, Hoogland S, Voznyy O, Zhitomirsky D, Debnath R, Levina L, Rollny L R, Carey G H, Fischer A, Kemp K W, Kramer I J, Ning Z, Labelle A J, Chou K W, Amassian A, Sargent E H. Hybrid passivated colloidal quantum dot solids. Nature Nanotechnology, 2012, 7: 577– 582
4. Li G, Zhu R, Yang Y. Polymer solar cells. Nature Photonics, 2012, 6 (3): 153–161
5. Chung I, Lee B, He J, Chang R P H, Kanatzidis M G. All-solid-state dye-sensitized solar cells with high efficiency. Nature, 2012, 485 (7399): 486–489
6. Debnath R, Bakr O, Sargent E H. Solution-processed colloidal quantum dot photovoltaics: a perspective. Energy & Environmental Science, 2011, 4(12): 4870–4881
7. Kramer I J, Sargent E H. Colloidal quantum dot photovoltaics: a path forward. ACS Nano, 2011, 5(11): 8506–8514
8. Tang J, Sargent E H. Infrared colloidal quantum dots for photovoltaics: fundamentals and recent progress. Advanced Materials (Deerfield Beach, Fla.), 2011, 23(1): 12–29
9. Hines M A, Scholes G D. Colloidal PbS nanocrystals with size-tunable near-infrared emission: observation of post-synthesis self-narrowing of the particle size distribution. Advanced Materials, 2003, 15(21): 1844–1849
10. Henry C H. Limiting efficiencies of ideal single and multiple energy gap terrestrial solar cells. Journal of Applied Physics, 1980, 51(8): 4494–4500
11. Wise F W. Lead salt quantum dots: the limit of strong quantum confinement. Accounts of Chemical Research, 2000, 33(11): 773–780
12. Brown A S, Green M A. Detailed balance limit for the series constrained two terminal tandem solar cell. Physica E, Low-Dimensional Systems and Nanostructures, 2002, 14(1–2): 96–100
13. Nozik A J, Beard M C, Luther J M, Law M, Ellingson R J, Johnson J C. Semiconductor quantum dots and quantum dot arrays and applications of multiple exciton generation to third-generation photovoltaic solar cells. Chemical Reviews, 2010, 110(11): 6873–6890
14. McDaniel H, Heil P E, Tsai C L, Kim K K, Shim M. Integration of type II nanorod heterostructures into photovoltaics. ACS Nano, 2011, 5(9): 7677–7683
15. Johnston K W, Pattantyus-Abraham A G, Clifford J P, Myrskog S H, MacNeil D D, Levina L, Sargent E H. Schottky-quantum dot photovoltaics for efficient infrared power conversion. Applied Physics Letters, 2008, 92(15): 151115
16. Luther J M, Law M, Beard M C, Song Q, Reese M O, Ellingson R J, Nozik A J. Schottky solar cells based on colloidal nanocrystal films. Nano Letters, 2008, 8(10): 3488–3492
17. Leschkies K S, Beatty T J, Kang M S, Norris D J, Aydil E S. Solar cells based on junctions between colloidal PbSe nanocrystals and thin ZnO films. ACS Nano, 2009, 3(11): 3638–3648
18. Barkhouse D A, Debnath R, Kramer I J, Zhitomirsky D, Pattantyus-Abraham A G, Levina L, Etgar L, Grätzel M, Sargent E H. Depleted bulk heterojunction colloidal quantum dot photovoltaics. Advanced Materials, 2011, 23(28): 3134–3138
19. Kramer I J, Zhitomirsky D, Bass J D, Rice P M, Topuria T, Krupp L, Thon S M, Ip A H, Debnath R, Kim H C, Sargent E H. Ordered nanopillar structured electrodes for depleted bulk heterojunction colloidal quantum dot solar cells. Advanced Materials, 2012, 24 (17): 2315–2319
20. Rath A K, Bernechea M, Martinez L, Konstantatos G. Solution-processed heterojunction solar cells based on p-type PbS quantum dots and n-type Bi_2 S_3 nanocrystals. Advanced Materials, 2011, 23 (32): 3712–3717
21. Rath A K, Bernechea M, Martinez L, de Arquer F P G, Osmond J, Konstantatos G. Solution-processed inorganic bulk nano-heterojunctions and their application to solar cells. Nature Photonics, 2012, 6(8): 529–534
22. Xu F, Ma X, Haughn C R, Benavides J, Doty M F, Cloutier S G. Efficient exciton funneling in cascaded PbS quantum dot superstructures. ACS Nano, 2011, 5(12): 9950–9957
23. Kramer I J, Levina L, Debnath R, Zhitomirsky D, Sargent E H. Solar cells using quantum funnels. Nano Letters. 2011, 11(9): 3701–3706
24. Liu H, Tang J, Kramer I J, Debnath R, Koleilat G I, Wang X, Fisher A, Li R, Brzozowski L, Levina L, Sargent E H. Electron acceptor materials engineering in colloidal quantum dot solar cells. Advanced Materials, 2011, 23(33): 3832–3837
25. Gao J, Luther J M, Semonin O E, Ellingson R J, Nozik A J, Beard M C. Quantum dot size dependent *J-V* characteristics in heterojunction ZnO/PbS quantum dot solar cells. Nano Letters, 2011, 11(3): 1002–1008
26. Gao J, Perkins C L, Luther J M, Hanna M C, Chen H Y, Semonin O E, Nozik A J, Ellingson R J, Beard M C. n-type transition metal oxide as a hole extraction layer in PbS quantum dot solar cells. Nano Letters, 2011, 11(8): 3263–3266
27. Brown P R, Lunt R R, Zhao N, Osedach T P, Wanger D D, Chang L Y, Bawendi M G, Bulović V. Improved current extraction from ZnO/PbS quantum dot heterojunction photovoltaics using a MoO_3 interfacial layer. Nano Letters, 2011, 11(7): 2955–2961
28. Jeong K S, Tang J, Liu H, Kim J, Schaefer A W, Kemp K, Levina L, Wang X, Hoogland S, Debnath R, Brzozowski L, Sargent E H, Asbury J B. Enhanced mobility-lifetime products in PbS colloidal quantum dot photovoltaics. ACS Nano, 2012, 6(1): 89–99
29. Klem E J D, Gregory C W, Cunningham G B, Hall S, Temple D S,

Lewis J S. Planar PbS quantum dot/C_{60} heterojunction photovoltaic devices with 5.2% power conversion efficiency. Applied Physics Letters, 2012, 100(17): 173109

30. Tang J, Kemp K W, Hoogland S, Jeong K S, Liu H, Levina L, Furukawa M, Wang X, Debnath R, Cha D, Chou K W, Fischer A, Amassian A, Asbury J B, Sargent E H. Colloidal-quantum-dot photovoltaics using atomic-ligand passivation. Nature Materials, 2011, 10(10): 765–771
31. Sargent E H. Infrared photovoltaics made by solution processing. Nature Photonics, 2009, 3(6): 325–331
32. Wang X, Koleilat G I, Tang J, Liu H, Kramer I J, Debnath R, Brzozowski L, Barkhouse D A R, Levina L, Hoogland S, Sargent E H. Tandem colloidal quantum dot solar cells employing a graded recombination layer. Nature Photonics, 2011, 5(8): 480–484
33. Choi J J, Wenger W N, Hoffman R S, Lim Y F, Luria J, Jasieniak J, Marohn J A, Hanrath T. Solution-processed nanocrystal quantum dot tandem solar cells. Advanced Materials, 2011, 23(28): 3144–3148
34. Koleilat G I, Wang X, Sargent E H. Graded recombination layers for multijunction photovoltaics. Nano Letters, 2012, 12(6): 3043–3049
35. Tang J, Wang X, Brzozowski L, Barkhouse D A R, Debnath R, Levina L, Sargent E H. Schottky quantum dot solar cells stable in air under solar illumination. Advanced Materials, 2010, 22(12): 1398–1402
36. Tang J, Brzozowski L, Barkhouse D A R, Wang X, Debnath R, Wolowiec R, Palmiano E, Levina L, Pattantyus-Abraham A G, Jamakosmanovic D, Sargent E H. Quantum dot photovoltaics in the extreme quantum confinement regime: the surface-chemical origins of exceptional air- and light-stability. ACS Nano, 2010, 4(2): 869–878
37. Luther J M, Gao J, Lloyd M T, Semonin O E, Beard M C, Nozik A J. Stability assessment on a 3% bilayer PbS/ZnO quantum dot heterojunction solar cell. Advanced Materials, 2010, 22(33): 3704–3707
38. Liu Y, Gibbs M, Perkins C L, Tolentino J, Zarghami M H, Bustamante J Jr., Law M. Robust, functional nanocrystal solids by infilling with atomic layer deposition. Nano Letters, 2011, 11(12): 5349–5355